

**Increased Actuation Rate of Electromechanical  
Carbon Nanotube Actuators Using Potential Pulses  
with Resistance Compensation**

**Joseph N. Barisci\*, Geoffrey M. Spinks, Gordon G. Wallace**

Intelligent Polymer Research Institute  
University of Wollongong  
NSW 2522  
Australia

**John D. Madden**

Department of Mechanical Engineering  
Massachusetts Institute of Technology  
Room 3-147, 77 Massachusetts Ave  
Cambridge MA 02139  
USA

**Ray H. Baughman**

NanoTech Institute  
University of Texas at Dallas  
Richardson, Texas 75083-0688  
USA

\* Corresponding author

Fax: 61 2 42213114

Email: [nbarisci@uow.edu.au](mailto:nbarisci@uow.edu.au)

**ABSTRACT**

The results of this study demonstrate that resistance compensation can provide significant improvement in the charging rate, and consequent actuation strain rate for carbon nanotube sheets operated in an organic electrolyte. The strain rate increased with increasing pulse amplitude and a more negative lower potential limit. The amount of strain produced also increased with longer pulse times. The highest strain rate achieved was 0.6 %/sec producing a strain amplitude of 0.3% in 0.5 sec. This performance is significantly better than previous reports. The improvements in strain rate are somewhat offset when large negative potential limits are used due to the introduction of Faradaic reactions in the electrolyte medium that do not contribute to actuation. Efficiency of operation is, therefore, reduced under such conditions. Some slight differences were observed between the negative and positive pulse directions, which are partly explained by the basic mechanism of actuation and partly by instrumental effects.

## INTRODUCTION

Recently, there has been considerable interest in electromechanical actuator materials that can be made to change shape by an electrical stimulus. Potential applications are many but include steerable catheters [1], an electronic Braille screen [2] and a prosthetic glove [3]. The ideal actuator material would operate at low voltage and at least match the performance of skeletal muscle: 10 % strain; 0.3 MPa stress generated; and 10 %/sec strain rate. Several low voltage actuator materials, including gels [4] and conducting polymers [5-12], are capable of meeting and even exceeding the first two requirements, but only high voltage electrostrictive elastomers [13] come close to matching the strain rate of natural muscle.

Single-wall carbon nanotubes (CNT) are potentially fast actuators because of their capacitive mechanism [14]. A porous sheet or paper of entangled CNT forms the working electrode of an electrochemical cell and application of a potential causes the formation of the electrical double layer at the electrode/electrolyte interface. The charge stored in the carbon atoms of the nanotubes is matched by the ionic charge on the liquid phase. However, the accumulated charge stored in the nanotube causes an increase in the C-C bond length during electron injection [14]. The rate at which bond length changes occur (and, hence, macroscopic actuation of the CNT sheet) is related to the rate of charge injection, which in turn, is related to ion transport rates in the electrolyte. This process, however, should be fundamentally faster than actuation in conducting polymers and hydrogels, where ions must diffuse through the bulk of the polymer to cause actuation. In CNT actuators, ion transport occurs through the electrolyte and is much faster than through bulk polymer films.

We have previously described extensively the electrochemical properties of CNT sheets [15-17] but the only data on actuation rates of CNT gives a maximum rate of  $\sim 0.5$  %/sec (having a strain amplitude of  $\sim 0.005\%$  in 10 msec)

[14]. In the present work, the slow actuation of CNT is assumed to result from electrolyte resistance. The aim of this study was to determine whether resistance compensation techniques are capable of increasing the rate of actuation in CNT sheets.

Resistance compensation techniques work by applying a higher input voltage to compensate for the ohmic ( $IR$ ) drop (product of current and resistance) that occurs across the electrolyte. The aim is to maximise the electrochemical potential at the electrode/electrolyte interface without causing degradation of the electrolyte or the electrode material. This aim can be achieved if the system is well modelled, allowing the double layer potential to be estimated. It is this potential that in turn determines the charge state of the CNT, and therefore the extent of actuation. With the double layer potential estimated, the input potential can be controlled (“shaped”) to maximize rate, while preventing excessive potential differences from developing across the double layer, and thereby avoiding degradation and overshoot [9,18].

One of the simplest cases where such an approach is desirable occurs when the electrolyte resistance is significantly greater than the electrode resistance. This is certainly the case for CNT in liquid electrolytes, and is well modelled using the approach described by Madden *et al.* for conducting polymer electromechanical actuators [9,18]. The nanotube actuator diffusion impedance ( $Z_D$ ) and double layer capacitance ( $C$ ) act as a low pass filter. The electrolyte resistance is then easily identified (*e.g.*, using an impulse, step or high frequency sinusoidal input). The  $IR$  then determines the potential drop across the electrolyte. Subtracting this potential from the total applied potential ( $E_a$ ) yields the double layer potential ( $E_{dl}$ ). Assuming that the double layer potential is meant to reach but not exceed a certain value ( $E_{dl}^{max}$ ) then the controller must simply maintain the input potential such that:

$$E_a = E_{dl}^{max} - IR \quad (1)$$

This method eliminates the rate-limiting effects of the electrolyte resistance ( $R$ ). The remaining rate limiting factors are then due to CNT resistance and mass transport.

Resistance compensation has been shown to be very effective in increasing actuation rate of polypyrrole actuators. Initially, we [9] demonstrated a peak strain rate of 3.4 %/sec, while more recently peak strain rates of up to 16 %/sec have been achieved using resistance compensation in combination with improved interconnects to overcome the resistance of polymer actuators [2]. In the present study we demonstrate that resistance compensation is also effective for increasing the actuation rate of CNT electromechanical actuators.

## **EXPERIMENTAL**

### **Chemical and Reagents**

Single-wall CNT dispersed in water or toluene were obtained from Tubes@Rice (Rice University) with purity better than 90%. The material consists of hexagonally packed bundles of nanotubes 1.2 to 1.4 nm in diameter. Each bundle consists of about 30-100 nanotubes, with an average diameter of 50-140 nm, and lengths of several micrometers [19]. Acetonitrile, silver perchlorate, tetrabutylammonium perchlorate (TBAP) and tetrabutylammonium hexafluorophosphate (TBAHFP) were supplied by Sigma.

### **Instrumentation**

A conventional three-electrode cell was used for all experiments. The working electrode was a piece (15 mm x 2 mm x 0.03 mm) of CNT paper attached to the potentiostat lead by a short piece of thin platinum wire, the reference electrode was Ag/Ag<sup>+</sup> (0.01 M AgClO<sub>4</sub>/0.1 M TBAP/acetonitrile), and the auxiliary electrode consisted of a piece of CNT paper several times larger than the working electrode. The potentiostat was a BAS CV-27 voltammograph. The output from the potentiostat was recorded using a MacLab 4e (ADInstruments) operated by Chart software (ADInstruments) and a Macintosh computer.

The potentiostat output is under computer control via a voltage input from a 12-bit digital to analog converter (D/A) on the National Instruments DAQ card 6024E. Voltages proportional to the working electrode/reference electrode potential difference and the current are read into the computer via two 12 bit analog to digital converters (A/D) on the same card. A custom compensation algorithm run in Microsoft Visual Basic 5 on an IBM Thinkpad 2611-552/Windows 98 makes use of measured current and voltage to control the applied potential. In this algorithm the user assigns double layer potential limits (corresponding to  $E_{dl}^{max}$ ), defined by  $E_U$  and  $E_L$ , and a potential step size,  $\Delta E$ . The potential of the working electrode (*vs* reference electrode) will never exceed  $E_B \pm \Delta E$ , where  $E_B$  is the potential of the working electrode measured immediately before applying a sequence of potential inputs. Once start has been signaled by the user, and the initial potential,  $E_B$ , has been measured, a step in potential,  $+\Delta E$ , is applied relative to  $E_B$ . The current and the potential of the working electrode are immediately recorded, from which the resistance,  $R$ , between the working and reference electrodes is estimated. Current,  $I$ , is continually measured and the  $IR$  drop calculated. When the condition:

$$(\Delta E + E_B) > E_U + IR \quad (2)$$

is met, the applied potential,  $\Delta E$ , is reset such that:

$$(E_B + \Delta E'(t)) = E_U + I(t)R \quad (3)$$

where  $t$  represents time. As the current tends to zero, the potential drop across the internal resistance also tends to zero, and the applied potential becomes  $E_U$ . After a specified time,  $-\Delta E$  is applied. Condition (2) and (3) are again in effect, with  $E_L$  replacing  $E_U$ . The feedback loop represented by Eqs. (2) and (3) runs 2250 times per second on average. The user specifies a number of cycles over which the algorithm is repeated.

Actuator testing used a beam balance apparatus as previously described [20]. The sample was fully immersed in the electrolyte solution and firmly fixed to the bottom of the electrolyte container. The top of the sample was attached to

one end of the balance beam and maintained under tension during testing by a small counter-weight at the other end of the beam (producing  $2g_f$  tension). A linear variable distance transducer (LVDT) was used to measure the deflection of the beam caused by sample contraction or expansion.

## Procedures

The fabrication of the CNT sheets has been previously described [13,19]. It involved vacuum filtration of the aqueous single-wall CNT suspension on a membrane filter, washing with water and methanol, air drying, and removal of the formed film from the filter. Removal of impurities from of the CNT sheets was carried out by thermal annealing under argon gas using the following temperature program: 20 to 120 °C at 20 °C/min, 120 °C for 2 h, 120 to 300 °C at 1 °C/min, 300 °C for 2 h, 300 to 600 °C at 5 °C/min, 600 to 1050 °C at 10 °C/min, 1050 °C for 1 h, cool to room temperature overnight.

The electrolyte solution (non-deoxygenated) was 0.2 M TBAHFP/acetonitrile. Resistance ( $R$ ) compensation was used during the application of potential pulses which consisted of a positive-going (P) step and a negative-going (N) step, with sizes  $+\Delta E$  and  $-\Delta E$ , respectively. The pulse parameters were,  $E_B$ : base potential,  $\Delta E$ : pulse amplitude,  $E_U$ : upper potential limit,  $E_L$ : lower potential limit,  $f$ : pulse frequency. These control parameters are defined in Fig. 1.

## RESULTS AND DISCUSSION

### Charging Tests

Initially, charging tests with potential pulses were conducted in a conventional electrochemical cell to check the software/hardware and to examine the effect of  $R$ -compensation. A typical result is presented in Fig. 2, which shows the application of a pulse with  $\Delta E$  of 1 V (U), 3 V (C) and 5 V (C) for the same  $E_L$  (-1 V). It can be seen clearly from Fig. 2c that the level and the rate of charging increases (2-10 times) when  $R$  is compensated and when  $\Delta E$  increases.

## Potential Ramps

Strain measurements using potential ramps typical of cyclic voltammetry were obtained in the actuation cell to establish the basic behaviour of the sample as a function of applied potential. A wide range of scan rates, 10-1000 mV/sec, was used. Typical curves for scans between -1.5 V and +0.5 V are given in Fig. 3. In the range between -1 V and 0.5 V the cyclic voltammograms do not exhibit any redox responses, typical of pure capacitive behaviour [15-17]. At more negative potentials, however, larger reduction currents are observed due probably to Faradaic reactions from dissolved oxygen, absorbed water or decomposition of the electrolyte. As a rule, the higher the scan rate the smaller the total amount of charge injected and the smaller the maximum strain generated. A 100-fold increase in scan rate reduces the maximum strain by 50 %. On the other hand, increasing scan rates produce strain-charge curves with greater slopes and smaller hysteresis. This is probably a consequence of Faradaic processes induced at negative potentials occurring to a lesser extent at faster scan rates. Similar data obtained using -1 V as negative potential limit showed strain-potential curves with similar trends but strain-charge curves with reduced hysteresis, consistent with smaller Faradaic currents. The overall parabolic shape of the strain-charge curves are consistent with the behaviour described by Baughman *et al.* [14].

## Potential Pulses

The effect of the various parameters used in the  $R$ -compensation technique ( $\Delta E$ ,  $E_L$ ,  $E_U$  and  $f$ ) on the strain response of the CNT sheets are described in Figs. 4-6. In each case, the potential-time profile is shown along with the resulting strain-time response for the N step followed by the P step. In addition, the strain is plotted as a function of the charge passed during each potential step. In most experiments,  $E_U$  was kept constant, usually at 0.5 V, while  $E_L$  was changed. This

approach was followed due to the fact that in CNT larger strain is generated at negative potentials [14].

#### *Effect of Pulse Amplitude ( $\Delta E$ )*

The effect of  $\Delta E$  on the actuation response is illustrated in Fig. 4. Improvements in both the strain magnitude and the rate (slope of linear part of strain-time curve) are obtained by increasing  $\Delta E$  from 2 to 3 V (Figs. 4a and 4c). Using  $R$ -compensation in comparison to the uncompensated potential pulse, produced gains in strain of up to 50 %. Pulse amplitudes higher than 3 V (4-10 V) produced a less significant advantage and are not included in the figures.

The expected strain-charge profile is approximately parabolic [14], reflecting the basic mechanisms of actuation occurring in CNT sheets. At extreme potentials Faradaic reactions can occur in the electrolyte that consume charge, but do not contribute to actuation strain. Previous work has shown that the applied potential should not exceed -1 V in TBAHFP/acetonitrile electrolyte to avoid Faradaic reactions [21].

As  $\Delta E$  increases, the net strain for a given charge is the same or improved, *e.g.*, see Fig. 4d in which the strain per charge is greater once charging is near completion but it is lower at small charge. When  $R$ -compensation is used, the double layer charges more rapidly and Faradaic reactions tend to increase as the potential is made more negative. Since more negative potentials are reached faster, there is initially more Faradaic component to the charge in the  $R$ -compensated case. However, since the compensated case reaches its final charged state faster, there is less time for Faradaic processes to occur. Beyond a certain charging level a cross-over is expected (as seen in Fig. 4d), where the compensated strain for a given charge level is higher than the value for the uncompensated case. The relationship between strain and charge (in the linear part of strain-charge curves) is typically  $1-2 \times 10^{-3} \text{ \%}/(\text{C/g})$ , or 50-100 C/g is needed to produce a 0.1 % strain.

### *Effect of Pulse Lower Limit ( $E_L$ )*

Making  $E_L$  more negative results in a significant increase in the magnitude and in the rate of the strain change (Fig. 5). The improvement in strain is more than 200% for an  $E_L$  change from -2 to -4 V. The maximum strain rate achieved is  $\sim 0.6$  %/sec which is the highest reported to date for carbon nanotubes. However, a possible disadvantage of using increasingly more negative  $E_L$  is that the rate of Faradaic processes increases, as shown by the lower strain-charge coefficients when  $E_L$  goes from -2 to -3 V (Fig. 5b). This additional charge and the resulting effect on the strain-charge relationship parallel those observed for potential ramps.

### *Effect of Pulse Frequency ( $f$ )*

The main effect of increasing  $f$  for a given set of  $R$ -compensated conditions is to reduce the strain (Fig. 6a). For a 60-fold increase in the frequency the maximum strain diminishes by about 10 times. The maximum strain rate practically does not change with increasing pulse frequency. The strain-charge relationships are also largely unchanged with increasing pulse frequency, with the exception that less charge is passed (and less actuation strain produced) when shorter pulses are used (Fig. 6b). The higher the frequency, the less time is available for double layer charging, and therefore the smaller the potential excursion.

### *Effect of Potential Step Direction (N/P)*

A characteristic feature of the measurements performed was that in most cases the P step produces a faster strain change than the N step, *i.e.*, contraction is faster than expansion (Figs. 4c, 5b, 6b). The difference, 5-150 % depending on experimental conditions, tends to become smaller, to the point of disappearing or even becoming inverted as  $\Delta E$ ,  $E_L$  or  $f$  increases. It seems that as the driving force increases in magnitude or rate of application, expansion benefits more than contraction while the system is less able to return to its initial state at  $E_U$  (drift). Also, the P step-induced strain has associated a lower and faster decaying current, a smaller charge and a steeper strain-charge curve than those

produced by the N step, suggesting a more efficient process. The parabolic shape of the strain-charge curve, exhibiting a relatively shallow minimum at  $\sim 0.4$  V [14], and the smaller Faradaic effects associated with the P step may account for the observed differences.

#### *Actuation Delay*

A common feature of the data collected is that a time delay ( $t_d$ ) is observed for the onset of actuation in relation to the charging. This delay can be seen by comparing the current-time curves with the strain-time curves but it is more clearly evidenced by the strain-charge plots. In all cases, at the beginning of the potential step a considerable amount of charge passes before a change in strain is observed. After this initial delay a relatively linear relationship exists between strain and charge until the electrode becomes practically fully charged.

The value of  $t_d$  does not appear to vary much with changes in the various parameters. The only clear difference occurs between the N step and the P step, with the latter having a  $t_d$  about 20-30 % shorter. Typical values of  $t_d$  are around 30-40 msec, time during which 5-20 % of the total charge has passed depending on experimental conditions. Although the parabolic strain-charge curve, with a minimum around 0.4 V, would predict for the N step the need to inject extra charge before strain is observed, this explanation does not account for the delay in the P step. A contribution to the delay undoubtedly arises from the inertia of the measuring system. The resonance frequency of the beam balance is estimated to be of the order of 30 Hz, meaning that the response time is approximately 15 msec. Thus,  $t_d$  appears to be caused by a combination of an instrument delay (for the N and P steps) and a delay caused by the strain-charge dependency (for the N step).

## CONCLUSIONS

The results of this study clearly demonstrate that resistance compensation can provide significant improvement in the charging rate, and consequent actuation strain rate for carbon nanotube sheets operated in an organic electrolyte. The strain rate increased with increasing pulse amplitude and a more negative lower potential limit. The amount of strain produced also increased with longer pulse times (although the pulse frequency did not affect strain rate). The highest strain rate achieved was 0.6 %/sec producing a strain amplitude of 0.3% in 0.5 sec. This performance is significantly better than previous reports (0.5%/sec strain rate with a strain amplitude of only 0.005%).

The improvements in strain rate are somewhat offset when large negative potential limits are used due to the introduction of Faradaic reactions in the electrolyte medium that do not contribute to actuation. Efficiency of operation is, therefore, reduced under such conditions.

Some slight differences were observed between the negative and positive pulse directions, which are partly explained by the basic mechanism of actuation and partly by instrumental effects.

**REFERENCES**

1. A. Della Santa, A. Mazzoldi and D. De Rossi, *J. Smart Mat. Syst. Struct.* **1999**, 7, 292-300.
2. J. Ding, L. Liu, G. M. Spinks, D. Zhou and G. G. Wallace, *Synth. Met.* **2002**, submitted for publication.
3. G. M. Spinks, G. G. Wallace, L. Liu and D. Zhou, *Proc. MRS* **2002**, in press.
4. Y. Osada and M. Hasebe, *Chem. Lett.* **1985**, 9, 1285-1288.
5. D. De Rossi and A. Mazzoldi, *Proc. SPIE-Int. Soc. Opt. Eng.* **1999**, 3669 (*Electroactive Polymer Actuators and Devices*), 35-44.
6. M. R. Gandhi, P. Murray, G. M. Spinks and G. G. Wallace, *Synth. Met.* **1995**, 73, 247-256.
7. K. Kaneto, M. Kaneko, Y. Min and A. G. MacDiarmid, *Synth. Met.* **1995**, 71, 2211-2212.
8. A. G. MacDiarmid, K. Kaneto, H. Saito and Y. Min, *Polym. Mater. Sci. Eng.* **1994**, 71, 713-714.
9. J. D. Madden, R. A. Cush, T. S. Kanigan and I. W. Hunter, *Synth. Met.* **2000**, 113, 185-192.
10. T. F. Otero and J. M. Sansinena, *Bioelectrochem. Bioenerg.* **1995**, 38, 411-414.
11. Q. Pei, O. Inganas and I. Lundstrom, *Smart Mat.* **1993**, 2, 1-6.
12. E. Smela, O. Inganas and I. Lundstrom, *J. Micromech. Microeng.* **1993**, 3, 203-205.
13. R. Pelrine, R. Kornbluh, Q. Pei and J. Joseph, *Science* **2000**, 287, 836-839.
14. R. H. Baughman, C. Cui, A. A. Zakhidov, Z. Iqbal, J. N. Barisci, G. M. Spinks, G. G. Wallace, A. Mazzoldi, D. De Rossi, A. Rinzler, O. Jaschinski, S. Roth and M. Kertesz, *Science* **1999**, 284, 1340-1344.
15. J. N. Barisci, G. G. Wallace and R. H. Baughman, *J. Electroanal. Chem.* **2000**, 488, 92.
16. J. N. Barisci, G. G. Wallace and R. H. Baughman, *Electrochim. Acta* **2000**, 46, 509.
17. J. N. Barisci, G. G. Wallace and R. H. Baughman, *J. Electrochem. Soc.* **2000**, 147, 4580.

18. J. D. Madden, P. G. Madden and I. W. Hunter, in *Proc. SPIE 8th Annual Symp Smart Struct. Mater: Electroact. Polym. Actuators and Devices*, Y. Bar-Cohen, Ed., (SPIE, Bellingham WA, 2001), pp. 72-83.
19. A. G. Rinzler, J. Liu, H. Dai, P. Nikolaev, C. B. Huffman, F. J. Rodriguesmacias, P. J. Boul, A. H. Lu, D. Heymann, D. T. Colbert, R. S. Lee, J. E. Fisher, A. M. Rao, P. C. Eklund, R. E. Smalley, *Appl. Phys. A* 29 (67) 1998.
20. G.M. Spinks, L. Liu, D. Zhou and G.G. Wallace, *Adv. Funct. Matl.* **2002**, 12, 437-440.
21. G.M. Spinks, G.G. Wallace, R.H. Baughman and L.M. Dai, "Carbon Nanotube Actuators", in *Electroactive Polymer Actuators*, edited by Y. Bar-Cohen (SPIE Press, Bellingham, Washington, 2001), pp. 223-246.

### **Acknowledgements**

This work was partially supported by US DARPA grant N00173-99-2000. R. H. Baughman acknowledges the partial financial support to the Robert A. Welch Foundation. G. G. Wallace acknowledges the continued support of the Australian Research Council.

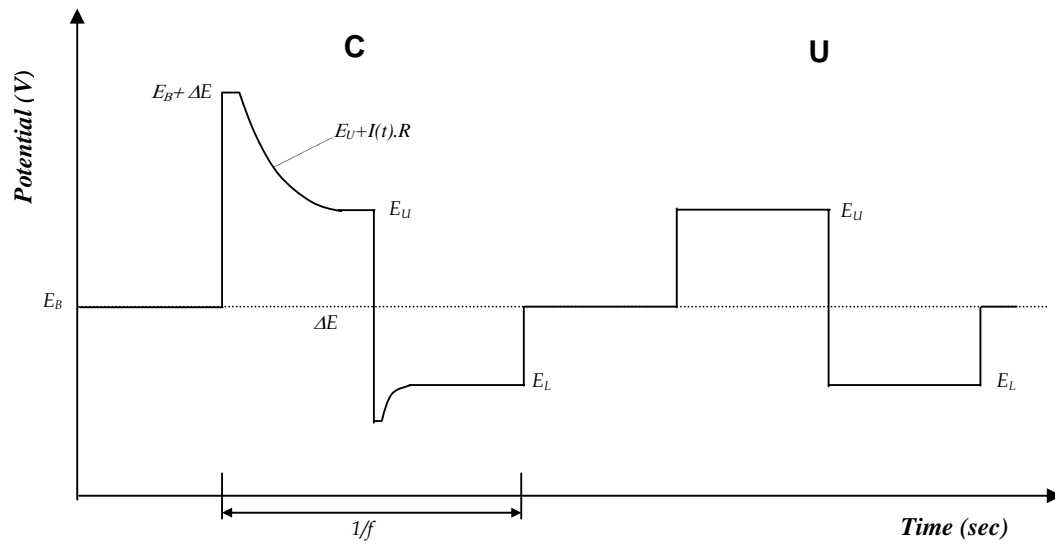


**Fig. 1:** Applied potential-time profile for a resistance compensated pulse (C) and an uncompensated pulse (U).

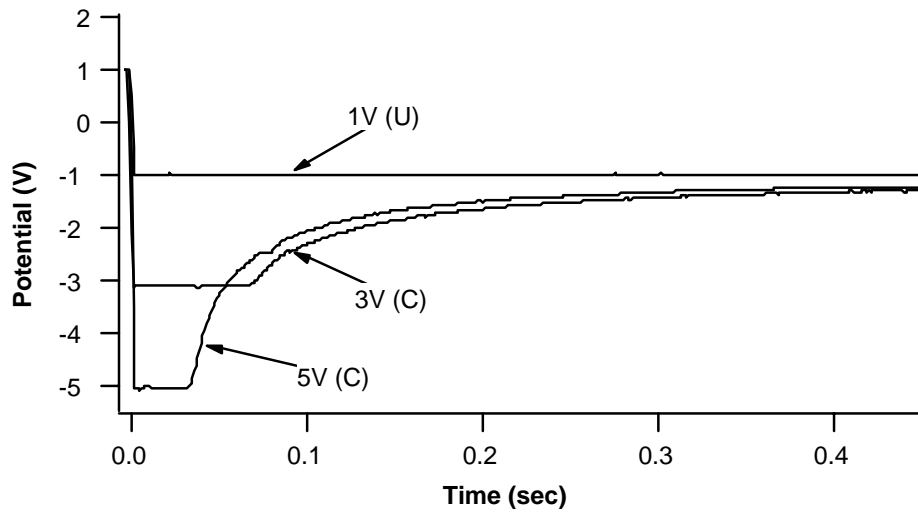


**Fig. 2a:** Potential-time curves for  $R$ -compensated (C) and uncompensated (U)  $N$  steps,  $E_B: 0\text{ V}$ ,  $E_U: 1\text{ V}$ ,  $E_L: -1\text{ V}$ ,  $f: 1\text{ Hz}$ ,  $\Delta E$ : as shown.

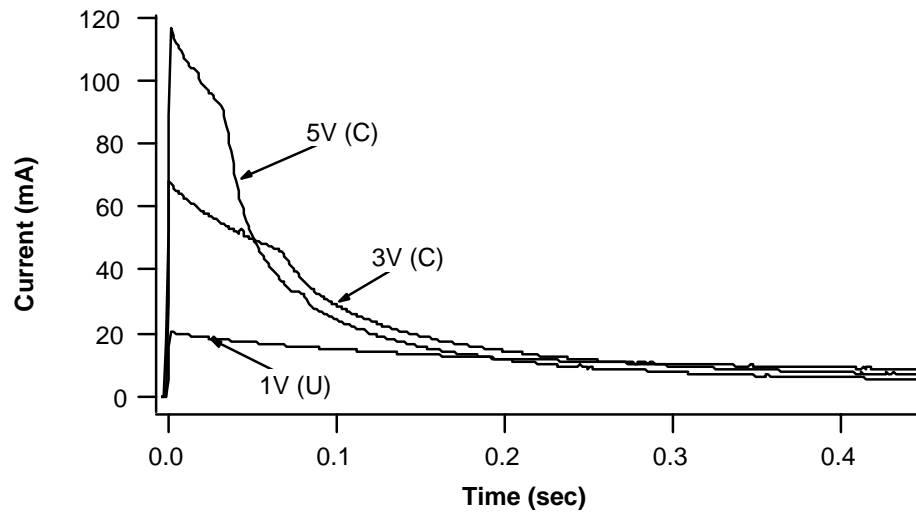


**Fig. 2b:** Current-time for  $R$ -compensated (C) and uncompensated (U)  $N$  steps (current shown with inverted sign),  $E_B: 0\text{ V}$ ,  $E_U: 1\text{ V}$ ,  $E_L: -1\text{ V}$ ,  $f: 1\text{ Hz}$ ,  $\Delta E$ : as shown.

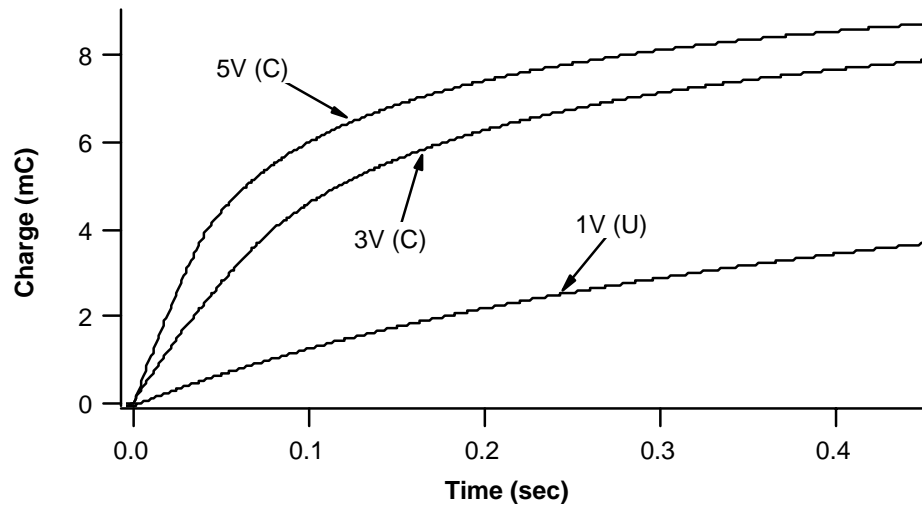


**Fig. 2c:** Charge-time for *R*-compensated (C) and uncompensated (U) *N* steps (charge shown with inverted sign),  $E_B: 0\text{ V}$ ,  $E_U: 1\text{ V}$ ,  $E_L: -1\text{ V}$ ,  $f: 1\text{ Hz}$ ,  $\Delta E$ : as shown.

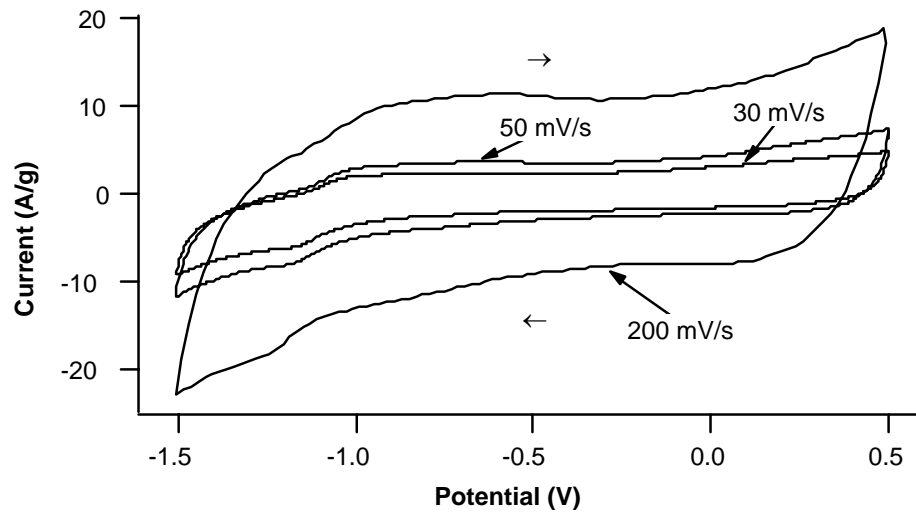


**Fig. 3a:** Current-potential curves for different scan rates,  $E_U$ : 0.5 V,  $E_L$ : -1.5 V, scan rate: as shown.

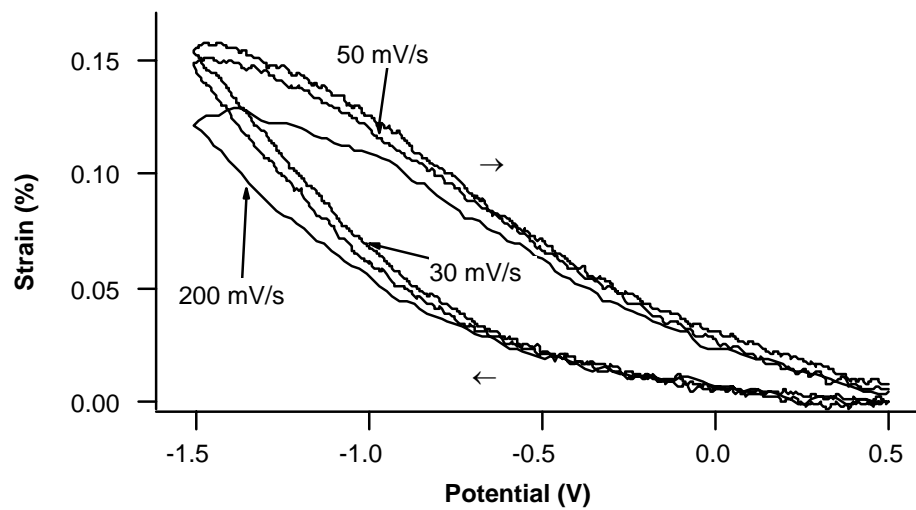


**Fig. 3b:** Strain-potential curves for different scan rates (in this and similar figs presented below expansion is shown as increasing strain),  $E_U$ : 0.5 V,  $E_L$ : -1.5 V, scan rate: as shown.

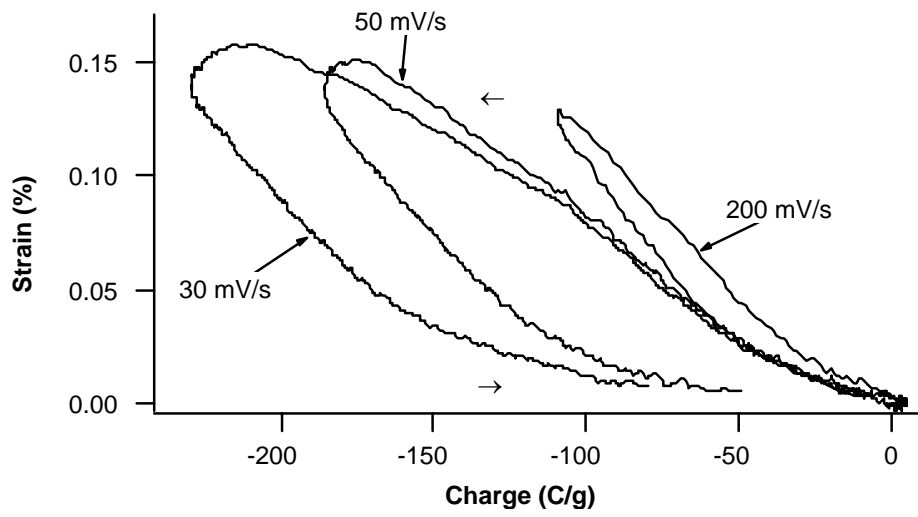


**Fig. 3c:** Strain-charge curves for different scan rates,  $E_U$ : 0.5 V,  $E_L$ : -1.5 V, scan rate: as shown.

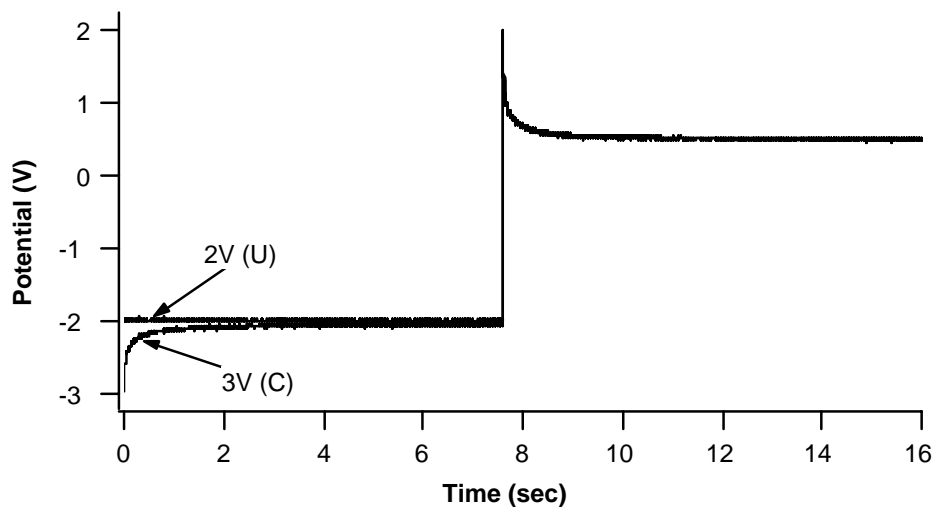


**Fig. 4a:** Potential-time curves for  $R$ -compensated (C) and uncompensated (U) pulses,  $E_B$ : 0 V,  $E_U$ : 0.5 V,  $E_L$ : -2 V,  $f$ : 0.06 Hz,  $\Delta E$ : as shown.

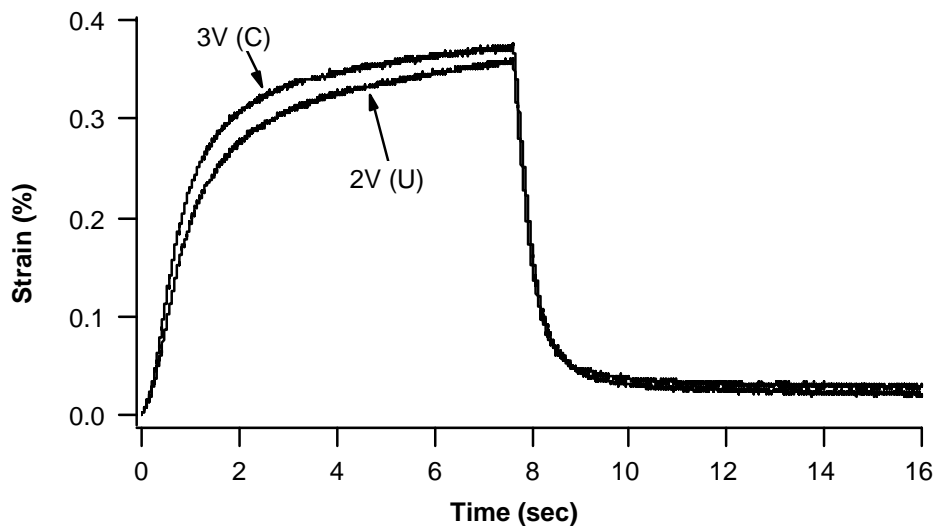


**Fig. 4b:** Strain-time curves for  $R$ -compensated (C) and uncompensated (U) pulses,  $E_B$ : 0 V,  $E_U$ : 0.5 V,  $E_L$ : -2 V,  $f$ : 0.06 Hz,  $\Delta E$ : as shown.

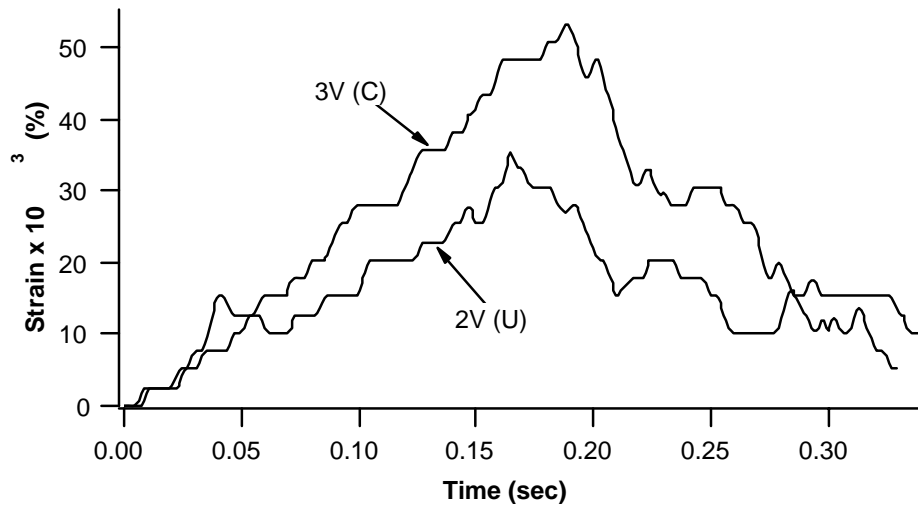


**Fig. 4c:** Strain-time curves for  $R$ -compensated (C) and uncompensated (U) pulses,  $E_B: 0$  V,  $E_U: 0.5$  V,  $E_L: -2$  V,  $f: 3$  Hz,  $\Delta E$ : as shown.

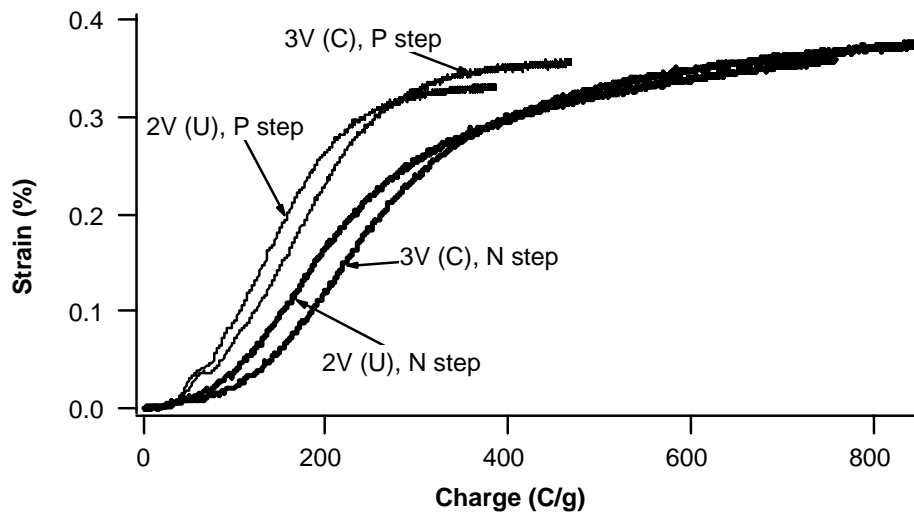


**Fig. 4d:** Strain-charge curves for  $R$ -compensated (C) and uncompensated (U) pulses,  $E_B: 0$  V,  $E_U: 0.5$  V,  $E_L: -2$  V,  $f: 0.06$  Hz,  $\Delta E$ : as shown (in this and similar figs presented below the P step strain-charge curves are shown inverted).

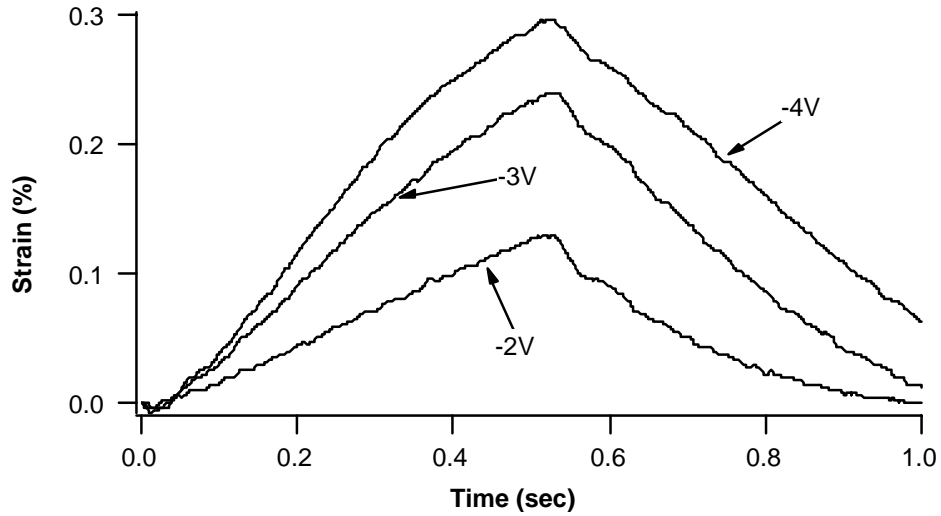


**Fig. 5a:** Strain-time curves for  $R$ -compensated pulses,  $E_B: 0\text{ V}$ ,  $E_U: 0.5\text{ V}$ ,  $\Delta E: 8\text{ V}$ ,  $f: 1\text{ Hz}$ ,  $E_L$ : as shown.

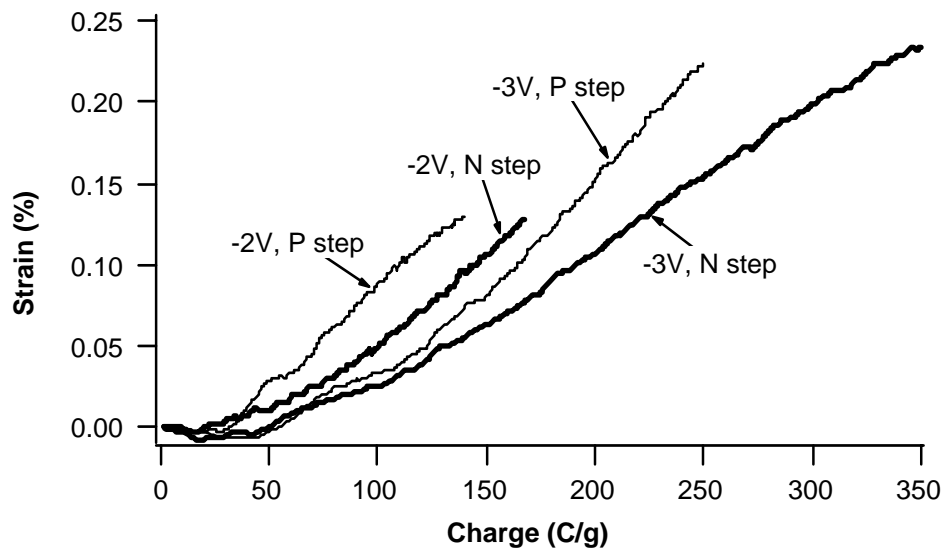


**Fig. 5b:** Strain-charge curves for  $R$ -compensated pulses,  $E_B: 0\text{ V}$ ,  $E_U: 0.5\text{ V}$ ,  $\Delta E: 8\text{ V}$ ,  $f: 1\text{ Hz}$ ,  $E_L$ : as shown.

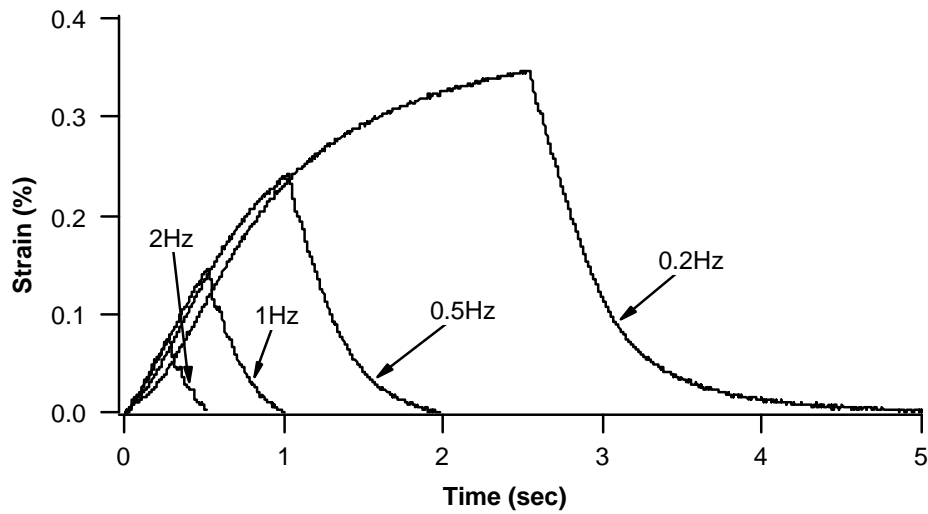


**Fig. 6a:** Strain-time curves for  $R$ -compensated pulses,  $E_B: 0\text{ V}$ ,  $E_U: 0.5\text{ V}$ ,  $E_L: -2\text{ V}$ ,  $\Delta E: 4\text{ V}$ ,  $f$ : as shown.

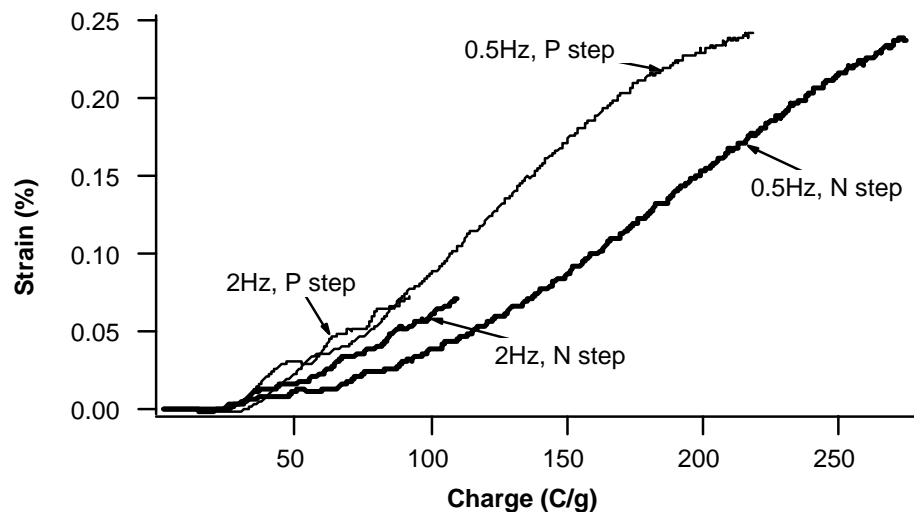


**Fig. 6b:** Strain-charge curves for  $R$ -compensated pulses,  $E_B: 0\text{ V}$ ,  $E_U: 0.5\text{ V}$ ,  $E_L: -2\text{ V}$ ,  $\Delta E: 4\text{ V}$ ,  $f$ : as shown.